Jpn. J. Appl. Phys. Vol. 41 (2002) pp. 1834–1837
Part 1, No. 3B, March 2002

Design and Fabrication of Fiberlenses for Optical Recording Applications

Chung-Hao TIEN*, Yin-Chieh LAI, Tom D. MILSTER[1] and Han-Ping D. SHIEH
Institute of Electro-Optical Engineering, National Chiao Tung University, Hsinchu, Taiwan 30010, R.O.C.
[1]*Optical Data Storage Center, Optical Science Center, University of Arizona, Tucson, Arizona 85711, U.S.A.*

(Received September 28, 2001; accepted for publication December 27, 2001)

The novel design and fabrication of a microlens on the front end of a single-mode fiber is described. The beam quality and spot size for optical recording applications are analyzed. A hyperbolic-shaped microlens on a single-mode fiber with focused spot of $1/e^2 = 0.82\,\mu$m (x-direction) and $0.89\,\mu$m (y-direction) at $\sim 145\,\mu$m working distance was achieved by a simple fabrication procedure. [DOI: 10.1143/JJAP.41.1834]

KEYWORDS: microlens, single-mode fiber, optical recording, thermal writing

1. Introduction

Optical disk systems are being developed with higher speed and density. Due to this trend, conventional lenses and their mountings with substantial mass will face difficulty regarding fast access motion. Moreover, tight tolerance in the optical path requirement limits the development of near-field optics using flying head systems.

Optical fibers have the advantages of low weight and high flexibility when used as light-guiding media. Fibers can overcome the tight tolerances found in high numerical aperture (*NA*) optical paths and can reduce the number of components, therefore reducing the cost and weight. Thus, fiber systems are a good choice for high-speed access that is to be applied in next-generation dynamic flying head systems in optical data storage.

Microlenses formed on the end of single-mode fibers (SMFs) are widely used for optoelectronic passive elements to faciliate laser-to-fiber coupling for optical communication systems. The objective of the coupling scheme is to (1) maximize the coupling efficiency and (2) minimize the optical feedback due to Fresnel reflection from fiber to laser. Several authors have proposed techniques for producing such end-of-fiber lenses as laser-to-fiber coupling elements.[1–6] These techniques include photolithography,[3] chemical etching,[4] mechanical polishing,[5] and thermal melting.[6] The lenses are minute in size, where the radius of curvature is only a few micrometers, and they have a short working distance of less than $10\,\mu$m.

Though these microlenses show fine performance, they are not adequate for use in optical scanning systems. First, these lenses require relatively cumbersome fabrication processes to ensure small microlens radius of curvature. Second, the minute working distance less than $10\,\mu$m can easily allow contact between the front edge of the microlens and the spinning disk. Finally, the short working distance between microlens and medium will result in high optical feedback due to Fresnel reflection from the lens front end, which will degrade the readout signal.

In this paper, we present a design and analyses of a fiber-front-end microlens used as a pick-up for optical data recording applications. The objective of our scheme is to achieve the smallest possible spot at a reasonable working distance.[7] The size of the focused spot for a thermal writing mechanism is directly related to the size of marks recorded on the medium. Also, the spot size determines the resolution of the system in the readout. A reasonable working distance is designed to avoid mechanical contact between the front end of microlens and the spinning disk.

2. Analyses

We designed a fiberlens with a large radius R compared to other published works.[1–6] The distance between the SMF and the microlens is filled with a pure silica rod of the same diameter and same refractive index as the core of the SMF to avoid reflection, as shown in Fig. 1. The mode field radius W_0 is computed by the following formula.[8]

$$\frac{W_0}{a} = 0.65 + \frac{1.619}{V^{3/2}} + \frac{2.879}{V^6}, \tag{1}$$

where a is the core radius of the step-index fiber, and V is the normalized frequency $V = \frac{2\pi}{\lambda_0} a\sqrt{n_1^2 - n_2^2}$ (n_1 and n_2, are the refractive indexes of core and cladding, respectively). The mode field diameter $2W_0$ at wavelength $\lambda_0 = 0.6328\,\mu$m is about $4.3\,\mu$m.

A hemispherical microlens at the front end is used as the focusing element. The length of the pure silica rod d is designed to control the focused beam waist W_i, which is defined as half-width at $1/e^2$ maximum intensity, and position Z_i, which is defined as the distance from the beam waist position to the lens front end. The relationships of W_i and Z_i as a function of propagation distance $g = d + R$, where R is the radius of the hemispherical lens, are shown in Fig. 2 under the

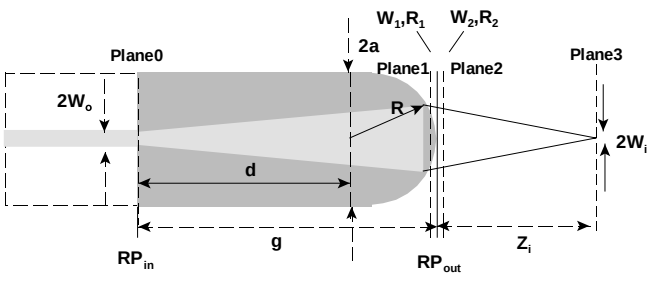

Fig. 1. Illustrated schematics of the microlens on the end face of the SMF (Refractive index of pure silica rod $n = 1.55$, cladding diameter $2a = 125\,\mu$m, mode field diameter $2W_0 = 4.3\,\mu$m of single-mode fiber at wavelength $\lambda_0 = 0.6328\,\mu$m).

*Email address: chtien.eo86g@nctu.edu.tw

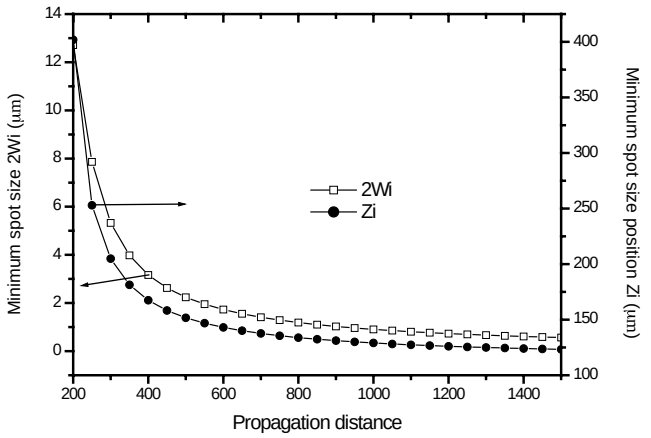

Fig. 2. Focused beam waist W_i and position Z_i decrease as propagation distance g increases under the paraxial approximation.

paraxial approximation (see Appendix A).

In our design, the beam continuously expands as it approaches the lens. If the mode field within the SMF is sufficiently small, the emitted beam in the silica rod exhibits a considerable divergence. In this case, the intensity of the incoming beam is expanded over the entire entrance aperture stop formed by the microlens rim. The focused beam then is distorted due to spherical aberration and an apodization effect. Using Fresnel diffraction integrals, the field distribution $I(r, z)$ at a distance z from the front end of the lens is expressed as,[9,10]

$$I(r,z) = \left| \frac{iA_1}{\lambda z} \exp\left(-ikz - \frac{ik}{2z}r^2\right) \int_0^D \rho J_0\left(\frac{k\rho}{z}r\right) \times \exp\left(-\rho^2\left\{\frac{1}{W_2^2} + \frac{ik}{2}\left[\frac{1}{z} + \frac{1}{R_2} + \frac{2\phi(\rho)}{\rho^2}\right]\right\}\right) \times d\rho \right|^2, \quad (2)$$

where D is the radius of the microlens circular aperture, W_2 and R_2 are the beam waist and the radius of curvature after passing through the end face of the silica rod (Plane 2), respectively, $\phi(\rho)$ is the third-order spherical aberration term of the hemispherical lens $\phi(\rho) = -\frac{1}{8}\frac{n^2(n-1)}{R^3}\rho^4$ (with radius of the lens curvature R, refractive index n), and k is the wave number in the silica rod. The focused beam is no longer a Gaussian distribution. Thus, we re-define the focused position as Z_p, where the beam has maximum on-axis intensity. The normalized field distribution at Z_p (a slight shift forward from Z_i) with different propagation distances g (300, 500, 800, and 1000 μm) are shown in Fig. 3, which are compared with ideal Gaussian beams at beam waist position Z_i under the paraxial approximation (dashed line). As shown in Fig. 3, the spherical aberration and truncation results in a short focal length shift and an increase in the size of the focused spot.

One way to compensate the wave aberration due to the hemispherical surface is to design an aspherical lens for a given radius of the hemispherical curve R.[6] The optical path length (OPL) passing through the (z, x) microlens surface

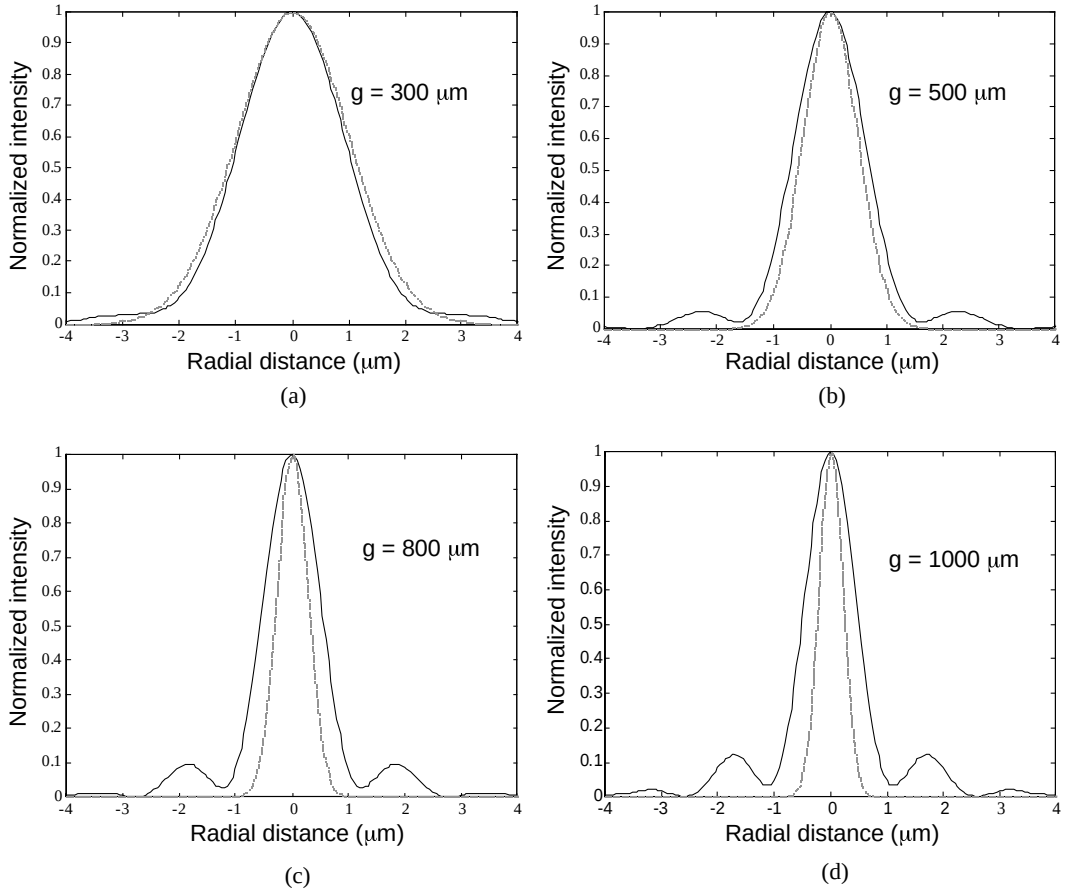

Fig. 3. Calculated normalized field distribution at different propagation distances g (μm). Solid line-at maximum on-axis intensity position Z_p by Fresnel diffraction integral; dashed-ideal gaussian beam at beam waist position Z_i by ABCD law.

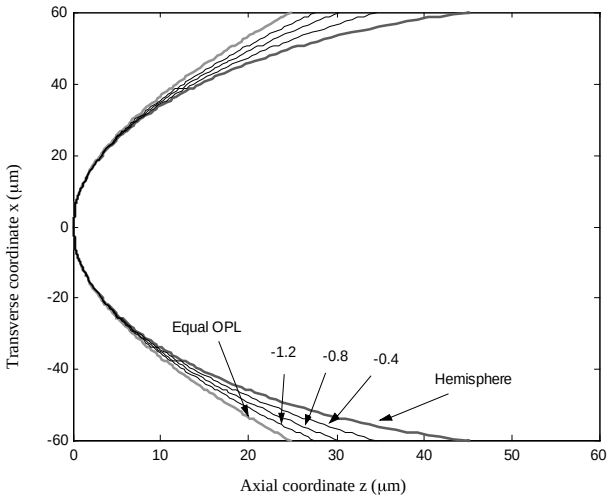

Fig. 4. Calculated hyperbolic shape with equal OPL from the light source to the designed focal length of fiberlens with $R = 62.5\,\mu$m compared with aspherical curve of different conic numbers ($K_c = -1.2, -0.8$, and -0.4) and hemispherical curve.

plane is given by:

$$\mathrm{OPL} = \sqrt{(Z_i - z)^2 + x^2} + n\sqrt{(g + z)^2 + x^2}, \qquad (3)$$

where Z_i and g are the designed working distance and silica rod length, respectively. The aspherical shape can be expressed as:

$$z = \frac{cx^2}{1 + \sqrt{1 - (1 + K_c)c^2x^2}}, \qquad (4)$$

where $c = 1/R$ is the curvature at the pole of the curve and K_c is the conic number. In the case of $g = 800\,\mu$m, $Z_i = 145\,\mu$m, and $R = 62.5\,\mu$m, the equal OPL curve from the source to the designed focal length is shown in Fig. 4, which is compared with different conic numbers of the aspherical shape. In this case, the curve is hyperbolic with the conic number $K_c \cong -1.8$.

3. Experiments and Discussion

3.1 Hemispherical-shaped microlens

Hemispherical microlenses are fabricated on the SMF front end by applying the high-frequency discharge arc method.[11,12] The fabrication process is schematically illustrated in Fig. 5 (steps (a)–(c)). First, we use an arc-discharge fiber splicer to join the SMF and a coreless fiber (silica fiber). Next, we cleave the pure silica fiber perpendicular to its axis and control the rod length d with the aid of a microscope eyepiece graticule. Then, we apply a high-frequency discharge arc. The free end of the silica rod contracts to form a hemisphere due to surface tension. A side view of the hemispherical lens is shown in Fig. 6(a). The focused spot size of the hemispherical microlens, shown in Fig. 6(b), is measured by imaging the focused spot onto the vidicon tube (PST-203, Kuge Precision Co., Ltd.) by a high numerical aperture objective lens.[13] In the case of $\lambda_0 = 0.6328\,\mu$m and propagation distance $g \cong 800\,\mu$m, the spot size at full-width of $1/e^2$ is $1.00\,\mu$m (x-direction) and $1.02\,\mu$m (y-direction).

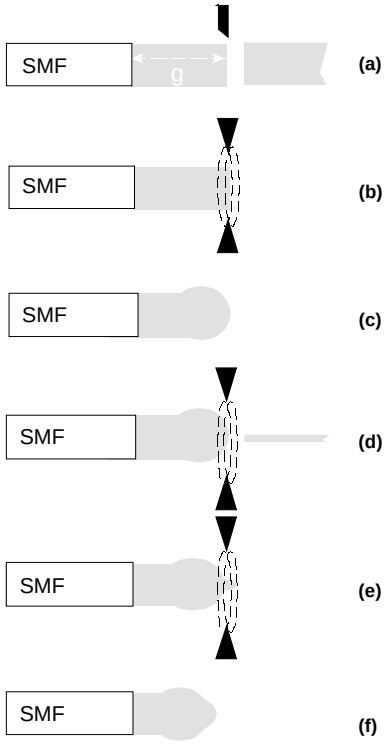

Fig. 5. Schematic illustration of the fabrication process for the hyperbolic-shaped fiberlens. (a) Pure silica rod perpendicular to their axes was cleaved to length g. (b) End face of the rod was heated by electric discharge. (c) End face of the rod contracts to form a hemisphere due to surface tension. (d) A droplet of pure silica on the lens front end. (e) Heated by an electric discharge arc again. (f) A hyperbolic-shaped microlens.

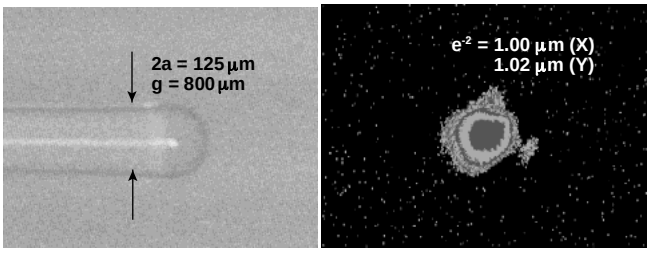

Fig. 6. (a) A side view of the hemispherical lens; (b) the measured spot size at full-width of $1/e^2$ is $1.00\,\mu$m (x-direction) and $1.02\,\mu$m (y-direction).

3.2 Hyperbolic-shaped microlens

Since the focused spot of the hemispherical-shaped microlens deteriorates due to spherical aberration, we investigate the compensated system that uses a hyperbolic-shaped microlens.[12] After achieving the hemisphrical surface, we tip a droplet of pure silica upon the lens front end, and then heat again using an electric discharge arc, as shown in Fig. 5 (steps (d)-(f)). Thus we can modify the hemispherical surface into a hyperbolic curve with a vertex radius ranging from 62.5 to $70\,\mu$m. The photograph shown in Fig. 7 was taken from the screen of the microscope of the splice machine. Figures 7(a) and 7(b) are photographs of the fiberlens at fabrication step (e) in Fig. 5, and a hyperbolic-shaped front end overlayed with a spherical curve of $62.5\,\mu$m (dashed line), respectively.

The hyperbolic-shaped lens can reduce the focused beam size and produce higher beam quality compared to a hemispherical-shaped microlens with similar parameters, as

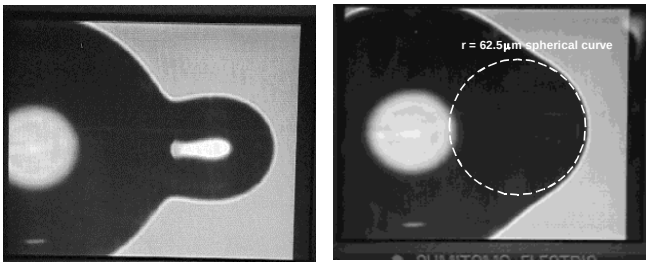

(a) (b)

Fig. 7. Photographs of (a) fiberlens at fabrication step (e) in Fig. 6 and (b) the hyperbolic-shaped front end overlayed with an $R = 62.5\,\mu$m spherical curve (dashed line).

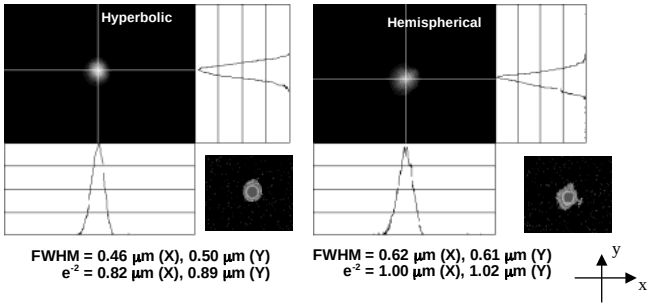

Fig. 8. Focused spot size of (a) hyperbolic-shaped and (b) hemispherical-shaped microlens.

shown in Fig. 8. Here, at wavelength $\lambda_0 = 0.6328\,\mu$m, the focused spot of full-width at $1/e^2$ is $0.82\,\mu$m (x-direction) and $0.89\,\mu$m (y-direction), for the hyperbolic microlens. The asymmetry of beam size is mainly due to the misalignment of the fabricated fiberlens surface to the optical axis.

4. Conclusions

We successfully designed and fabricated a hyperbolic-shaped microlens on a single-mode fiber to achieve the focus spot of $1/e^2 = 0.82\,\mu$m (x-direction) and $0.89\,\mu$m (y-direction) at $\sim 145\,\mu$m working distance using a simple fabrication procedure. This microlens design is easily compatible with other optical components to achieve micr-optical integration. The microlens is now being applied to thermal writing and as a readout mechanism in optical data storage applications.

Acknowledgement

This work was supported by the Ministry of Education of the Republic of China under contract with the Academic Center of Excellence in "Photonics Science and Technology for Tera Era" under contract No. 89-E-FA06-1-4.

1) L. Cohen and M. Schneider: Appl. Opt. **13** (1974) 89.
2) C. Edwards, H. Presby and C. Dragone: J. Lightwave Technol. **11** (1993) 252.
3) K. S. Lee and F. S. Barnes: Appl. Opt. **24** (1985) 3134.
4) G. Eisenstein and D. Vitello: Appl. Opt. **21** (1982) 3470.
5) H. Sakaguchi, N. Seki and S. Yamamoto: Electron. Lett. **17** (1981) 425.
6) J. I. Yamada, Y. Murakami, J. I. Sakai and T. Kimura: IEEE J. Quant. Electron. **16** (1980) 1067.
7) K. Shiraishi, N. Oyama, K. Matsumura, I. Ohishi and S. Suga: J. Lightwave Tech. **13** (1995) 1736.
8) D. Marcuse: Bell Syst. Tech. J. **56** (1976) 703.
9) K. S. Lee: Appl. Opt. **25** (1986) 3671.
10) J. W. Goodman: *Introduction to Fourier Optics* (McGraw-Hill, New York, 1968).
11) G. D. Khoe, J. Poulissen and H. M. de Vrieze: Electron. Lett. **19** (1983) 205.
12) W. Bludau, and R. H. Rossberg: J. Lightwave Tech. **3** (1985) 294.
13) W. T. Anderson and D. L. Philen: J. Lightwave Tech. **1** (1983) 10.

Appendix

The schematic of the lens is shown in Fig. 1. For the thick microlens system by ABCD law, W_1 and R_1, beam waist and radius at output plane RP_{out} (Plane 1) can be expressed as

$$W_1 - W_0\sqrt{1+\left(\frac{g}{Z_{\text{R}}}\right)^2} \tag{A·1}$$

and

$$R_1 = g + \frac{Z_{\text{R}}^2}{g}, \tag{A·2}$$

where W_0 is the mode field radius of an SMF, g is the propagation distance from RP_{in} (Plane 0) to RP_{out}, and Z_{R} is the Raileigh range where

$$Z_{\text{R}} = \frac{\pi W_0^2 n}{\lambda_0}. \tag{A·3}$$

After passing through the end face of the silica rod, the radius of curvature R_2 at Plane 2 becomes

$$R_2 = \frac{R_1 f}{f - R_1}, \tag{A·4}$$

where f is the focal length under paraxial approximation given by

$$f = \frac{R}{1-n}(R\langle 0,\ f\rangle 0), \tag{A·5}$$

and R is the radius of the plano convex lens on the fiber front end.

Thus, the focused beam waist W_{i} and working distance Z_{i} can be written as

$$W_{\text{i}} = \frac{W_2}{\sqrt{1+\left[\dfrac{\pi W_2^2}{\lambda R_2}\right]^2}} \tag{A·6}$$

and

$$Z_{\text{i}} = \frac{-R_2}{\sqrt{1+\left[\dfrac{\lambda R_2}{\pi W_2^2}\right]^2}}, \tag{A·7}$$

respectively.